Fabrication of efficient organic and hybrid solar cells by fine channel mist spray coating

By *Jae-hyeong Lee*[1], *Susumu Yoshikawa*[2] and *Takashi Sagawa*[1]

[1]Graduate School of Energy Science, Kyoto University
Yoshida-honmachi, Sakyo-ku, Kyoto 606-8501 (Japan)

[2]Institute of Advanced Energy, Kyoto University
Gokasho, Uji, 611-0011 Kyoto (Japan)

e-mail: sagawa.takashi.6n@kyoto-u.ac.jp

Keywords: organic thin-film solar cell, inverted solar cell, hybrid solar cell, bulk heterojunction, spray coating

Three types of organic and hybrid photovoltaics, which include poly (3-hexylthiophene) (P3HT), [6, 6]-phenyl C61 butyric acid methyl ester (PCBM) and zinc oxide (ZnO) in their active layer as normal, inverted and hybrid solar cells, were prepared by fine-channel mist–spray coating in air. In particular, we investigated the donor/acceptor blending effect for increasing reproducibility in normal type, annealing temperature control for more effective ZnO layer in inverted type solar cells. Patterns of sparse and vertical distribution by solvent polarity were discussed in fabrication for hybrid solar cells. Consequently, enough blending of donor/acceptor solution, the combination of pre/post heat treatment for ZnO layer and trade-off relation between crystallization of ZnO and ordering of the P3HT matrix were factors to be considered for enhanced results in terms of high photovoltaic performance.

1. Introduction

Organic photovoltaics (OPV) is fast emerging potential renewable, lightweight, large area and low-cost solar cell technology [1-12]. One of the most famous bulk heterojunction (BHJ) OPV structures is the device based on the composites of poly (3-hexylthiophene) (P3HT) as an electron donor and [6, 6]-phenyl C61 butyric acid methyl ester (PCBM) as an electron acceptor [13-16]. Recently, the power-conversion efficiency of state-of-the-art in polymer

solar cells (PSCs) has exceeded 10 % [17, 18]. These remarkable evolution of performance has made stimulated the progress more and more actively.

For normal devices using aluminum as a cathode, degradation takes place by diffusion of oxygen and water through the electrode. Long-term stability is another critical problem because poly (3, 4-ethylenedioxythiophene):poly(styrene sulfonate) (PEDOT:PSS) used as an anode buffer layer is hygroscopic and acidic [19-24]. In addition, it has been reported that a vertically uneven distribution of donors and acceptors in BHJ disturbs charge transport in conventional PSCs [25, 26]. One approach to overcome this issue is using inverted structure where the charge collection is reversed. The degradation in interface of ITO/PEDOT:PSS does not happen and the inverted structure employs stable and less air sensitive electrode material with high work function. Sol-gel derived ZnO film, which has high electron mobility, environmental stability and high transparency, is widely applied for inverted solar cells [27-30].

Organic-inorganic hybrid solar cells are focused on the advantage obtained with the inorganic acceptor materials, which have stability in environment [31], complimentary light absorption [32, 33], photogeneration of charge carriers [34, 35], quantum confinement effect [36] with low cost device production [2]. Well-controlled nanorod or nanofiber structure provide electron transporting pathways and efficient excitonic dissociation with blocking recombination.

To fabricate these three types of solar cells, multiple methods have been developed by many research groups. Spin-coating is the general fabrication method in the research field of organic solar cells (OSCs). The spin-coating method has been widely used in laboratories, due to its high precision and reproducibility. However, there is inherently a large amount of waste of materials in spin-coating and it is not compatible with roll to roll or large area manufacturing. Among the other solution processes recently used for the fabrication of OSCs, such as screen printing [37], doctor blading [38], inkjet printing [39, 40], and spray process

[41-47], the spray process is considered as one of the most promising. This is largely due to the fact that the spray coating process can be done at high production speed and is compatible with various substrates since the sprayed droplets are transferred from the spray nozzle to the substrate without direct contact with the surface. Also, the spray process allows for patterning of the coated film at a sub-millimeter scale with the use of shadow masks. In addition, the spray process can facilitate much more dilute solutions than the spin-coating method, allowing for the use of various organic materials that have poor solubility in solvents [48].

Recently, the implementation of the modified spray-mist coating technology for fabrication of an organic-based bulk heterojunction solar cell was reported [26]. The modified spray-mist coating method utilizes atomized droplets by ultrasonic generator, which is commonly known as a commercial ultrasonic humidifier or diffuser. It is plausible to be applied for large scale fabrication of polymer based solar cells. In addition, the modified spray-mist coating technology allows to pattern on the targeted area easily. This is critical, for instance, for fabricating a monolithic photovoltaic device that is integrated and connected to one large module. Another characteristic of this modified spray-mist coating method is a simple coating method, in which the liquid solution is ultrasonically atomized and the aerosol droplets are transferred onto the substrate by carrier gas. In our experiment, the fine channel mist deposition process consists of the donor and/or acceptor spray coating by gas pressure without chemical reaction of the precursors. Therefore, well-controlled deposition is expected to be produced a reproducible morphology in fabricating active layers, electron transport layers and hole transport layers. Moreover, this apparatus can blend droplets with different polarity. That is why carried droplets are not emitted out into the air instantly, but once reserved and mixed before being sprayed. It can be meaningful that simple and direct coating for mass production is actualized. Moreover, it is possible to avoid complicated preparation and procedures for ZnO nanoparticles and nanorods in hybrid solar cells. However, inevitable heat treatment for stable coating and limitation of size of droplets emitted should be considered before applying

to fabrication in solar cells. In this report, on the basis of optical morphology and topography, we investigated required considerations to fabricate a well-performed various typed solar cells of normal, inverted, and hybrid types, respectively.

2. Experimental

In the preparation of solar cell devices, indium-tin-oxide (ITO) coated glass substrates (Geomatec, 5 Ω cm^{-2}) were first patterned by etching and then cleaned thoroughly with a sequence of solvents: detergent, deionized water, acetone and isopropanol, for 10 min each in an ultrasonic bath. The cleaned substrates were purified further by oxygen plasma treatment for 10 min. The ultrasonic transducer produces vibration with 6 oscillators in the water. The solution was atomized by the ultrasonic transducer (2.9 MHz) and the aerosols formed were transferred with the nitrogen carrier gas at a flow rate of 4 L min^{-1}. The mixed aerosols in the nozzle were finally supplied through the linear source nozzle onto the heated substrate at a rate of 1.2 mL min^{-1}. The substrate temperature and number of coating exposures were controlled after the surface morphology investigation in the pretest, adapting for experiments. The stage was moved at a constant rate of 1 mm s^{-1}. The distance of the nozzle from the substrate was 1 mm.

For normal type solar cell, we prepared thin films and solar cell active layers based on a 1:0.8 mixture of P3HT (Rieke Metal) and PCBM (Nano C) dissolved in chlorobenzene (CB) by the fine-channel mist-spray deposition (FCMSD). Solutions of the active layer components, P3HT and PCBM, were prepared separately with a concentration of 8 mg mL^{-1} in CB and stirred in ultrasonic bath at 50 °C for 2 h. These solutions of active layer components were each loaded to its corresponding ultrasonic bottle for mist generation. For FCMSD (MIX) coating, P3HT and PCBM dissolved in CB respectively were blended for 40 min. An additional solvent mist spray coating was done by spraying *o*-dichlorobenzene (DCB) onto

the active layers at a rate of 100 μl min^{-1} at ambient temperature. The active layer was then allowed to dry for about 10 s. For the spray coating process as a reference, the airbrush (XP-727, Airtex Co., Ltd.) was powered by N_2 gas at 70 psi, a relatively low pressure that ensures fine atomization and prevents blowing off the droplets already deposited on the substrate. The solution was also prepared based on a 1:0.8 mixture of P3HT (Rieke Metal) and PCBM (Nano C) dissolved in CB. The distance of the airbrush from the substrate was 10 cm. An additional solvent spray coating was done by spraying DCB onto the active layers for 1 min at a rate of about 100 μl min^{-1}. The substrate was kept at atmospheric condition during all spray coating process. Before active layer coating, the substrates were then spin coated with a 0.45 μm filtered PEDOT:PSS solution (Clevios P), purchased from HC Starck, at 4000 rpm for 60 s to produce a 40 nm thick layer. The substrates were subsequently heated on a hotplate in air at 200 °C for 10 min to remove excess water. An additional solvent mist spray coating was done by spraying DCB onto the active layers at a rate of 100 μL min^{-1} at ambient temperature. The active layer was then allowed to dry for about 10 s.

For the inverted solar cell, the starting solution used was zinc acetate dehydrate, $Zn(CH_3COOH)_2 \cdot 2H_2O$, diluted at 0.02 mol L^{-1} in a solvent, where the volume ratio of methanol:water mixture is 4:1. Zinc acetate precursor directly contact on the substrate heated at 90, 120, 150, 180 and 210 °C. All devices are post-heated at 250 °C for 6 min after pre-heated coating. The thickness of ZnO layer was around 60-80 nm. Active layer coating was performed as method for normal type solar cell. For efficient FCMSD coating, PEDOT:PSS was mixed with water with a volume ratio of 1:3.

In hybrid system, zinc acetate dehydrate, $Zn(CH_3COOH)_2 \cdot 2H_2O$, was diluted at 0.069 mol L^{-1} in a solvent, where the volume ratio of methanol:water mixture is 40:1. The amount of water was minimized for reproducibility in organic-inorganic solar cell. Solutions of the

P3HT was prepared with a concentration of 10 mg mL^{-1} in CB and stirred in ultrasonic bath at 50 °C for 2 h.

Thermal annealing was performed at 150 °C in a glove box. Lithium fluoride (1 nm), molybdenum trioxide (5 nm), aluminum (100 nm) and silver (100 nm) were deposited by thermal evaporation in ultra-high vacuum at 5×10^{-3} Pa. The photovoltaic characteristics were measured under nitrogen atmosphere using an Agilent 4156C parameter analyzer under AM1.5G (100 mW cm^{-2}) simulated illumination using a solar simulator with a 1000 W xenon arc lamp.

For device characterization, the thickness was measured using an Alpha-Step IQ surface profiler of KLA-Tencor Co. which has a precision of ±10 nm. The surface image was measured with a Wyko NT9100 optical profilometry.

UV–visible absorption spectra were obtained using a Shimadzu UV-1601PC UV–visible spectrophotometer. Thin polymer films were deposited onto previously cleaned quartz slides with the same settings used for the production of solar cells.

To investigate the effect of the additional solvent sprayed on the morphology of the active layer, X-ray Diffraction (XRD) and surface profiler were used. The morphology of the active layer was observed by Transmission electron microscopy (TEM) (JEM2100).

Field-emission scanning electron microscope (FE–SEM, SU6600) and Energy Dispersive Spectroscopy (EDS) was used for investigating the distribution of components.

3. Results and Discussion

3.1 Normal type solar cell

Figure 1 shows a schematic illustration of the FCMSD apparatus in our experiment [26]. Flow rate is controlled by carrier gas (N_2). Donor (P3HT) and acceptor (PCBM) solutions are changed to tiny droplets in two separate mist sources. Fog or mist from two sources is

transferred seperately to nozzle along plastic tube. Heated substrate moves on the stage repeatedly and accurately. Device performance of the deposited films was investigated based on common device configuration: glass-ITO/PEDOT:PSS/P3HT:PCBM/LiF/Al. The film is formed by spreading of droplets and combining of adjacent droplets. The film morphology usually depends on the solution in the mist sources such as vapor pressure, boiling point, surface tension as well as flux of the droplets and ambient conditions [41-45, 47, 49]. In the FCMSD method, the flux of the solution is the most influential factor because of the short distance between the nozzle and the substrate. In our experiment, the moving substrate was kept at 110 ℃ to allow the active layer to have the better morphology. Many droplets are accumulated rapidly and led to liquid phase below 100 ℃. The high temperature enables the quality of the layers to be reproducible and under control. Even though this high drying temperature affect badly to formation of an well-established crystallite in the active layer [42, 50-52], the damage can be recovered by DCB additional solvent coating [26, 47]. The DCB additional solvent coating leads to dissolve the uneven and rough surface, which was attributed to fast drying.

To look into the morphology of the surface after FCMSD coating, we investigated the surface of a specific area, where Al was coated. The Al on the back reflects the light and shows the some defect and pin-hole on the surface easier. Even though DCB additional solvent coating was sprayed, the perfect layer without pin-holes is hardly obtained, considering the principle of being coated on the substrate. In this respect, we should take into account the optimal thickness, for both transportation of carriers and prevention of defects. Because the active layer is formed by the accumulation of dried droplets, an optimal active layer is comparatively thick. Too thin active layer cannot cover pinholes and cracks, which are formed by dried droplets [53, 54]. In addition to the thicker active layer, the additional DCB coating is applied to build proper carrier path and connect the isolated droplets. Finally,

it was found that the minimum thickness of the active layer for stable and reproducible performance was around 300 nm after the additional DCB solvent coating. In previous report, we found the optimal thickness of active layer can be variable according to the main coating process [54].

In **Figure 2**, we compared a current density-voltage (*J-V*) characteristic and incident photon-to-current efficiency (*IPCE*) of three devices with different coating method. Among the two devices by the FCMSD method, one utilizes only a single channel for blended P3HT/PCBM (triangle - FCMSD (MIX)) and the other one is fabricated by two separate channels for each donor and acceptor (rectangle - FCMSD). It is compared by spray coated device with same structure and thickness (a broken line). The device fabricated from two separate channel (FCMSD) has open circuit voltage (V_{oc}) = 0.54 V, current density (J_{sc}) = 6.75 mA cm^{-2}, fill factor (*FF)* = 0.56 and efficiency (*Eff*) = 2.03 %. Notably, the *J-V* characteristic of the device used one single channel (FCMSD (MIX)) (V_{oc} = 0.57 V, J_{sc} = 8.02 mA cm^{-2}, *FF* = 0.60 and *Eff* = 2.75 %) are superior to the performance of a spray coated device with a non-heated substrate by an airbrush. This value is also compatible to the performance of spin coated one in air, even if it is not shown here but reported previously[47]. It is thought that the additional DCB solvent annealing method compensate for losses, which would result from a hot substrate. It is found that the devices fabricated by FCMSD (MIX) have the maximum *IPCE* at 560 nm, broader peak between 500 nm and 650 nm of wavelength compared to spray coated device.

Figure 2 (a), (b) show that the two channels system is not enough to blend the donor and acceptor totally in the space of nozzle. Moreover, the low electrical characteristic in two channels system may come from the unbalanced deposition caused by the density gap of donor and acceptor. It is known that the density of PCBM (1.50 g cm^{-3}) is higher than the one of P3HT (1.10 g cm^{-3}) [55, 56]. The PCBM has better solubility in CB than P3HT, so the dried PCBM droplets are lifted up by a rising current air from the hot substrate. It leads to the

vertical distribution of P3HT and PCBM in the coating process [26]. Finally, this phenomenon restricts the formation of proper BHJ nanostructure. Accordingly, when this FCMSD is used for active layer deposition, it should be considered that degradation may happen due to imperfect blending and property of donor/acceptor materials. Neverdeless, this FCMSD is still more effective and attractive in the way that each donor/acceptor dissolved with even different solvents could be coated under a well-controlled manner.

3.2 Inverted type solar cell

The surface properties of zinc actate/ZnO films on glass substrates were investigated by a surface profiler and an optical microscope. The topography and optical images (inset) are respectively depicted in **Figure 3**. The topography by the surface profiler are obtained over 93.8 μm x 125.1 μm scanning range. Zinc acetate precursor directly contact on the substrate heated at 90, 120, 150, 180 and 210 °C. Using zinc acetate as a precursor, the acetate groups as contaminants of the gel decompose under annealing producing combustion volatile by-products [57]. The temperature of substrate, which is pre-heat treatment, is one of the most prominent factors in growth orientation of ZnO. The orientation of crystallites changes under the influence of solvent evaporation and existence of organic compounds. Therefore, the optimum pre-heat temperature is controlled, according to the solvent and additives. Usually, the temperature above 300 °C is required to produce (002) oriented films in the case of 2-methoxythanol and monoethanolamine [58, 59]. However, low pre-heat temperature also achieved good results recently in solvent of 2-methoxythanol (200 °C), 2-propanol (100 °C) and methanol (80 °C) [60-62]. In FCMSD deposition for ZnO thin film, zinc acetate dehydrate diluted in a methanol-water mixture which produce aerosol particles easily and evaporate quickly. To confirm the relation between the pre-heat and the post-heat treatment temperatures, all devices are post-heated at 250 °C for 6 minutes after pre-heated coating. The

character of (H) in Figure 3 represents the post-heating process. Surface profiler and optical images shows smooth films when pyrolysis happened at above 150 °C. When only pre-heat treatment below 120 °C is performed, the speed of removal of solvent does not catch up the speed of emission from nozzle and consequently some traces of undried excess solvent are left with rough morphology on the surface. Even at 150 °C, the ZnO precursor film gave a poorly or uniquely patterned morphology with high height differences. This morphology like patterned-print was also found in previous report [29]. Interestingly, post-heat treatment at 250 °C changed remarkably both morphology and topography, especially in the case of the devices prepared through pre-heat treatment at 120, 150 and 180 °C. It is attributed that the solvent vaporization, zinc acetate decomposition and zinc oxide crystal growth occur in entire layer as post-heat treatment proceeds. Significant change of optical images in inset of Figure 3 supports these facts. The pinholes left during pre-heat treatment at 90 °C come from insufficient coating by too low temperature than boiling point of the solvent. On the contrary, large agglomeration at 210 °C is caused by too quick vaporization of methanol-water mixture. XRD characterization of ZnO pyrolyzed at various temperature as pre-heat or post-heat treatment was investigated in **Figure 4**. The thermodynamically stable crystal structure of ZnO is wurtzite, which exhibits strong diffraction peaks at 2θ values of 31.8 ° (100), 34.5 ° (002) and 36.3 ° (101). There is no typical peak in the films coated between 90 °C and 180 °C as pre-heat treatment. Because the strange peak at 2θ values of 33.9 ° found at low pre-heat treatment disappears after post-heat treatment at 250 °C, it is considered that the peak originates from organic compounds resulting from incomplete decomposition of the metal-organic source. Weak crystalline ZnO peaks start to appear during pre-heat treatment at 210°C and the typical peaks shows no enhancement after post-heat treatment. This shows that optimized temperature as pre-heat treatment leads to pyrolysis and induce to form crystalline ZnO simply without post-heat treatment [30]. The reason of the (002) higher peak at 120°C

(H) is not clear here because the orientation of the ZnO thin film is sensitively dependent on various parameters as Zn concentration, solvent, additive and aging time [27, 28, 64]. Simply taking account of the pre-heated temperature as only parameter, a pre-heated process at 120 °C favors a preferred crystal orientation along (002) plane. The pre-heat temperature seems to be more critical factor for obtaining (002) orientation at least because there is no remarkable change at typical peak by post-heat treatment after the pre-heated treatment from 150 °C to 210 °C [60, 65, 66].

UV- vis absorption spectra in **Figure 5** indicates what process is more significant factor for ZnO pyrolysis during the heat treatment. To form ZnO through only pre-heat treatment, higher temperature above 180 °C is required, as shown in Figure 5. In addition, the effect of post-heat treatment after pre-heat treatment at high temperature is limited, comparing each absorbance in the region between 300 nm and 370 nm of 210 °C (solid, red) and 210 °C (H) (dotted, red). An additional consideration with these experimental results before deciding the optimum heat process is that the too high pre-heat treatment affect the quality of surface in repeated process of FCMSD. In other words, ZnO formed very fast adheres to the nozzle and disturb effective coating between the nozzle and substrate. Consequently, formation of ZnO at 150 °C (H), which is combined with pre-heat at 150 °C and post-heat at 250 °C, is promising for electron transport layer in inverted OSC.

In order to investigate the application of ZnO as an electron transport layer in inverted OSC, we fabricated two inverted structure devices of ITO/ZnO(F)/P3HT:PCBM(S)/MoO_3(E)/Ag(E) and ITO/ZnO(F)/P3HT:PCBM(F)/PEDOT:PSS(F)/Ag(E) and compared the *J-V* characteristics as shown in **Table 1**. The abbreviation of F, S and E means FCMSD method, spin coating, evaporation respectively. **Figure 6** shows representative *J-V* characteristics and *IPCE*s of the two devices. It shows the performance of the inverted type is better than that of normal typed device having ITO/PEDOT:PSS(S)/P3HT:PCBM(S)/LiF(E)/Al(E), compared to the results as shown in Figure 2. This fact exhibits that ZnO layer was stably formed by the

FCMSD method at relatively low temperature. The second device for roll-to-roll continuous coating, which is fabricated by FCMSD method as much as possible, shows degradation of *J-V* characteristic, especially *FF*. Although the factors affecting *FF* have not been completely identified yet, it has generally been accepted that *FF* is derived from the morphology of the active layer, charge-carrier transport, the balance between hole and electron mobility, and the interface of layers in OSC [65]. The degradation of *FF* also means increased R_s and decreased R_{sh}, as shown Figure 6. Heterogeneous and voided surface by consecutive FCMSD coating process leads to inferior contact among three interlayers. The contact resistance between interlayers affects the increment of R_s more significantly than the resistance of the ZnO, P3HT:PCBM, PEDOT:PSS layer itself [67]. For devices comprising only ZnO film by FCMSD, the maximum *IPCE* is 65 % in Figure 6 (b), which is indicative of efficient photon-to-elctron conversion. It is thought that the performance of ZnO layer in inverted type solar cell fabricated by FCMSD is limited particularly by the morphology and the extent of the contact between ZnO layer and active layer at the interface with active layer.

2.1 Hybrid type solar cell

Figure 7 shows optical images of surface coated with P3HT/ZnO. Considering that polar and non-polar solvent coexist in the state of droplets, perfect blending in the nozzle is actually not expected. Note that any nanorods and nanoparticles were not applied here. Generally, the ZnO nanorods and nanoparticles in hybrid solar cells play an important role in providing percolating pathways and carrier separation on ZnO/organic semiconductor. To achieve original purpose that the FCMSD was designed for speedy and simple mass production, the additional enhancement by nanostructures was excluded on purpose. Additionally, relatively low temperature unlike in inverted type solar cell was examined because high temperature annealing is not compatible with organic semiconductors. When the temperature of pre-heat

treatment is below 120 °C, uneven distribution of P3HT (red color) and ZnO (gray color) is found, as shown in Figure 7 (a), (b). This trend is somewhat avoided through controlled pre-heat treatment at 150 °C, drying the solvents including P3HT and ZnO effectively as shown in Figure 7 (c). However, hot substrate rapidly evaporates methanol-water mixture mixed solvent, and makes the formation of ZnO not on the substrate but near the nozzle as described above. Unfortunately, this phenomenon is distinguished in repeated process to get an optimal thickness of the active layer. In that case, bad morphology and agglomeration of donor/acceptor affects exciton diffusion and charge separation negatively. The additional DCB solvent coating can relieve bad morphology [47], however, extra DCB in the domain of ZnO remains on the surface as shown in Figure 7 (d).

TEM was carried out to investigate the morphology of the thin film. TEM image of the domain of P3HT and ZnO constituting the thin film is shown in **Figure 8**. It reveals that its own domain of P3HT and ZnO is formed independently, not showing heterogeneous interblending in tens of nanometer. Closer inspection in Figure 8 (b) also shows that the boundary exists between donor and acceptor. It is attributed to the each solvent with different property, namely polar (methanol) and non-polar (CB). Generally, the large droplet can then collide with small droplet and combine to form even larger drops in the nozzle. However, the two different polar droplets are not blended enough and each droplets are separately emitted out. This implies that the boundary between ZnO and P3HT may appear and consequently donor-acceptor are separated in the active layer. In Figure 8, ZnO shows up as the darker regions due to a consequence of a higher electron density. ZnO is not homogenously dispersed inside the polymer matrix. In this case, exciton dissociation at donor/acceptor interface seldom happens. Larger of P3HT domains than the exciton diffusion lengths (~10 nm) of the polymer means that recombination occurs easily and charge extraction is limited.

Figure 9 shows the distribution of sulfur (S) and zinc (Zn) in P3HT/ZnO active layer, measured by EDS on the Scanning Electron Microscopy (SEM). In EDS of P3HT/ZnO active

layer, sulfur comes from P3HT, which means that we can estimate the distribution of P3HT by dots of sulfur. The spatial distribution of S and Zn in P3HT/ZnO active layer was further analyzed by the observation of cross-sectional views with EDS technique. For clearer observation, the active layer was coated repeatedly until the thickness of active layer reached to 10 μm. We found that the distribution of S is unbalanced and abundant near the bottom of the layer as shown in Figure 9 (b). Analogous phenomenon was found in previous report [26]. This phenomenon can be explained as follows: Zn acetate precursor dissolved in methanol dries faster when aerosol emits. Subsequently, ZnO lifted up by ascending air current cover P3HT repeatedly. In particular, this trend occurred readily as the thickness of active layer increases. However, this phenomenon is improved partly when DCB additional coating is performed effectively in active layer of thickness below 300 nm.

Figure 10 (a), (b) show UV-vis absorption spectra of P3HT, ZnO and the blend of P3HT:ZnO films through the coating on the ITO substrate at 100, 150 (heat treatment during 6 min after the coating at 100 °C), and at 180 °C. When the P3HT exist only, the vibronic absorption shoulder at 550 nm and 600 nm become larger as the temperature goes up. However, the remarkable increase of the absorption in the region of 320-360 nm ascribed to ZnO is observed in the ZnO film through the post-annealing at 150 °C for 6 min. In contrast, the peak intensity of ZnO pre-heated at 180 °C without post-annealing is not strong. It means that the extent of pyrolysis of zinc acetate need to enough time and high temperature. Because the starting solution includes excessive methanol for coating effectively, the formation reaction of ZnO quickly happens in the state of vapor before the ZnO precursors reach to the high-temperature substrate. However, this phenomenon is weakened by existence of non-polar solvent like CB as shown in Figure 10 (b). CB with high boiling point suppresses the evaporation of methanol and induces to contact onto substrate for pyrolysis of zinc acetate. In coating process by blending P3HT:ZnO droplets, the increment of relatively large-sized ZnO hinders the formation of highly ordered lamella by disrupting the interchain interactions

between P3HT chains, resulting in decrease of intensity and vibronic shoulders between 500 nm and 550 nm as shown in Figure 10 (b). In addition, the spectrum of P3HT in the P3HT/ZnO composite film resulted in a blue shift from 520 nm (100 °C) to 500 nm (180 °C) with increasing pre-heated temperature. It is caused by the fast formation of ZnO at high temperature, which evokes to disordering of P3HT interchains.

Table 2 summarizes *J-V* characteristics of P3HT/ZnO hybrid solar cells with different post-treatment. In this experiment, it is hard to obtain ZnO below 150 °C within short coating time. However, too high temperature should be avoided because the fast removal of the solvent CB like in FCMSD prevents the formation of highly ordered lamella by disrupting the interchain interactions between P3HT chains [68-71]. Therefore, we applied the solvent additional coating to disordered P3HT domain through all of the devices 1-4. Interestingly, V_{oc} and E_{ff} decrease sharply in device 2, which is applied by heat treatment after DCB solvent coating. It is thought that unabsorbed DCB in domain of ZnO prevent removal of residual organic compounds. This estimation is confirmed by the increased efficiency of device 3, where heat treatment is performed before DCB solvent annealing. However, repeated and longer heat treatment is negative to the performance as shown in device 4.

Consequently, the trade-off between crystallization of ZnO and ordering of the P3HT matrix regarding to temperature of heat treatment should be reflected in fabrication of hybrid solar cell. In addition, the DCB solvent annealing is recommended to be performed after heat treatment in order to remove residual organic compounds in ZnO more effectively.

4. Conclusion

We have investigated the critical factors to apply the three types of solar cells through new coating process with the FCMSD technique. The experiments were proceeded to overcome against limitations such as use of a heated substrate and difficulty of detail manipulation on

process, maintaining advantages of the FCMSD method as like well-controlled mass production. Fully enough blending donor/acceptor solution is required to obtain a comparable and reproducible performance in normal type solar cell. In inverted type device, the combination of pre and post heat treatment (at 150 °C and 180 °C, respectively) induced better crystallization of ZnO. As a result, vertical distribution and trade-off between ordering of P3HT and growth of ZnO happened in the way of applying the FCMSD to hybrid solar cells directly. We expect this new technique will be an all-around alternative process for large scaled manufacturing production as well as various types of solar cells, keeping in mind the discussed factors.

Acknowledgements

The authors are indebted to Prof. Yoshinobu Tsujii and Assoc. Prof. Kohji Ohno of Institute for Chemical Research, Kyoto University for the use of the surface profiler and TEM, Prof. Toshinobu Yoko and Assoc. Prof. Yomei Tokuda for the use of XRD. They thank to Prof. Takeshi Yao and Assoc. Prof. Takeshi Yabutsuka of Graduate School of Energy Science, Kyoto University for the use of the SEM. They are also grateful to Dr. Yoshio Masuda (TOUKI Co. Ltd.) for his advice on the design and manufacturing of the FCMSD apparatus. This work is partially supported by the New Energy and Industrial Technology Development Organization (NEDO) of the Ministry of Economy, Trade, and Industry (METI), Core Research of Evolutional Science & Technology Agency (CREST) from Japan Science Technology Agency (JST), and the Global Center of Excellence (GCOE) Program of Kyoto University from the Ministry of Education, Culture, Sports, Science and Technology (MEXT) in Japan.

References

[1] K. Norrman, M. V. Madsen, S. A. Gevorgyan, F. C. Krebs, Degradation Patterns in Water and Oxygen of an Inverted Polymer Solar Cell, Journal of the American Chemical Society 132 (2010) 16883–16892.
[2] Y. Liu, T. T. Larsen-Olsen, X. Zhao, B. Andreasen, R. R. Søndergaard, M. Helgesen, K. Norrman, M. Jørgensen, F. C. Krebs, X. Zhan, All polymer photovoltaics: From small inverted devices to large roll-to-roll coated and printed solar cells, Solar Energy Materials and Solar Cells 112 (2013) 157–162.
[3] S. Günes, N. S. Sariciftci, Hybrid solar cells, Inorganica Chimica Acta 361 (2008) 581–588.
[4] H. Hoppe, N. S. Sariciftci, Polymer Solar Cells, Advances in Polymer Science 214 (2008) 1–86.
[5] B. R. Saunders, M. L. Turner, Nanoparticle–polymer photovoltaic cells, Advances in Colloid and Interface Science 138 (2008) 1–23.
[6] F. C. Krebs, Fabrication and processing of polymer solar cells: A review of printing and coating techniques, Solar Energy Materials and Solar Cells 93 (2009) 394–412.
[7] T. Ameri, G. Dennler, C. Lungenschmie, C. J. Brabec, Organic tandem solar cells: A review, Energy & Environmental Science 2 (2009) 347-363.
[8] B. Kippelen, J.-L. Brédas, Organic photovoltaics, Energy & Environmental Science 2 (2009) 251-261.
[9] J. Peet, A. J. Heeger, G. C. Bazan, 'Plastic' Solar Cells: Self-Assembly of Bul Heterojunction Nanomaterials by Spontaneous Phase Separation, Accounts of Chemical Research 42 (2009) 1700–1708.
[10] I. Gonzalez-Valls, M. Lira-Cantu, Vertically-aligned nanostructures of ZnO for excitonic solar cells: a review, Energy & Environmental Science 2 (2009) 19-34.
[11] B. C. Thompson, J. M. J. Fréchet, Polymer–Fullerene Composite Solar Cells, Angewandte Chemie International Edition 47 (2008) 58–77.
[12] C. N. Hoth, S. A. Choulis, P. Schilinsky, C. J. Brabec, On the effect of poly(3-hexylthiophene) regioregularity on inkjet printed organic solar cells, Journal of Materials Chemistry 19 (2009) 5398-5404.
[13] G. Li, V. Shrotriya, J. Huang, Y. Yao, T. Moriarty, K. Emery, Y. Yang, High-efficiency solution processable polymer photovoltaic cells by self-organization of polymer blends, Nature Materials 4 (2005) 864–868.
[14] J. Y. Kim, K. Lee, N. E. Coates, D. Moses, T.-Q. Nguyen, M. Dante, A. J. Heeger, Efficient Tandem Polymer Solar Cells Fabricated by All-Solution Processing, Science 317 (2007) 222–225.
[15] G. Dennler, M. C. Scharber, C. J. Brabec, Polymer-Fullerene Bulk-Heterojunction Solar Cells, Advanced Materials 21 (2009) 1323–1338.
[16] H. Hoppe, N. S. Sariciftci, Morphology of polymer/fullerene bulk heterojunction solar cells, Journal of Materials Chemistry 16 (2006) 45-61.
[17] J. You, C.-C. Chen, Z. Hong, K. Yoshimura, K. Ohya, R. Xu, S. Ye, J. Gao, G. Li, Y. Yang, 10.2% Power Conversion Efficiency Polymer Tandem Solar Cells Consisting of Two Identical Sub-Cells, Advanced Materials 25 (2013) 3973–3978.
[18] J. You, L. Dou, K. Yoshimura, T. Kato, K. Ohya, T. Moriarty, K. Emery, C.-C. Chen, J. Gao, G. Li, Y. Yang, A polymer tandem solar cell with 10.6% power conversion efficiency, Nature Communications 4 (2013) 1446.
[19] K. Kawano, R. Pacios, D. Poplavskyy, J. Nelson, D. D. C. Bradley, J. R. Durrant, Degradation of organic solar cells due to air exposure, Solar Energy Materials and Solar Cells, 90 (2006) 3520–3530.

[20] M. P. de Jong, L. J. van Ijzendoorn, M. J. A. de Voigt, Stability of the interface between indium-tin-oxide and poly(3,4-ethylenedioxythiophene)/poly(styrenesulfonate) in polymer light-emitting diodes, Applied Physics Letters 77 (2000) 2255.
[21] H. Yan, P. Lee, N. R. Armstrong, A. Graham, G. A. Evmenenko, P. Dutta, T. J. Marks, High-Performance Hole-Transport Layers for Polymer Light-Emitting Diodes. Implementation of Organosiloxane Cross-Linking Chemistry in Polymeric Electroluminescent Devices, Journal of the American Chemical Society 127 (2005) 3172–3183.
[22] K. Norrman, S. A. Gevorgyan, F. C. Krebs, Water-Induced Degradation of Polymer Solar Cells Studied by $H_2{}^{18}O$ Labeling, ACS Applied Materials & Interfaces 1 (2009) 102–112.
[23] J.-C. Wang, C.-Y. Lu, J.-L. Hsu, M.-K. Lee, Y.-R. Hong, T.-P. Perng, S.-F. Horng, H.-F. Meng, Efficient inverted organic solar cells without an electron selective layer, Journal of Materials Chemistry 21 (2011) 5723-5728.
[24] K. W. Wong, H. L. Yip, Y. Luo, K. Y. Wong, W. M. Lau, K. H. Low, H. F. Chow, Z. Q. Gao, W. L. Yeung, C. C. Chang, Blocking reactions between indium-tin oxide and poly (3,4-ethylene dioxythiophene):poly(styrene sulphonate) with a self-assembly monolayer, Applied Physics Letters 80 (2002) 2788.
[25] Z. Xu, L.-M. Chen, G. Yang, C.-H. Huang, J. Hou, Y. Wu, G. Li, C.-S. Hsu, Y. Yang, Vertical Phase Separation in Poly(3-hexylthiophene): Fullerene Derivative Blends and its Advantage for Inverted Structure Solar Cells, Advanced Functional Materials 19 (2009) 1227–1234.
[26] J. Lee, T. Sagawa, S. Yoshikawa, Fast Screening of the Optimal Polymer Ratio for Organic Solar Cells Using a Spray-Coating Deposition Method for the Fullerene Mixture, Energy Technology 1 (2013) 85–93.
[27] X.-H. Wang, J. Shi, S. Dai, Y. Yang, A sol-gel method to prepare pure and gold colloid doped ZnO films, Thin Solid Films 429 (2003) 102–107.
[28] Y.-S. Kim, W.-P. Tai, S.-J. Shu, Effect of preheating temperature on structural and optical properties of ZnO thin films by sol–gel process, Thin Solid Films 491 (2005) 153–160.
[29] T. Kuwabara, T. Nakashima, T. Yamaguchi, K. Takahashi, Flexible inverted polymer solar cells on polyethylene terephthalate substrate containing zinc oxide electron-collection-layer prepared by novel sol–gel method and low-temperature treatments, Organic Electronics 13 (2012) 1136–1140.
[30] Y.-J. Noh, S.-I. Na, S.-S. Kim, Inverted polymer solar cells including ZnO electron transport layer fabricated by facile spray pyrolysis, Solar Energy Materials and Solar Cells 117 (2013) 139–144.
[31] S. Ren, L.-Y. Chang, S.-K. Lim, J. Zhao, M. Smith, N. Zhao, V. Bulović, M. Bawendi, S. Gradeč ak, Inorganic–Organic Hybrid Solar Cell: Bridging Quantum Dots to Conjugated Polymer Nanowires, Nano Letters 11 (2011) 3998–4002.
[32] S. Dayal, N. Kopidakis, D. C. Olson, D. S. Ginley, G. Rumbles, Photovoltaic Devices with a Low Band Gap Polymer and CdSe Nanostructures Exceeding 3% Efficiency, Nano Letters 10 (2010) 239–242.
[33] N. C. Nicolaidis, B. S. Routley, J. L. Holdsworth, W. J. Belcher, X. Zhou, P. C. Dastoor, Fullerene Contribution to Photocurrent Generation in Organic Photovoltaic Cells, The Journal of Physical Chemistry C 115 (2011) 7801–7805.
[34] Y. Zhou, M. Eck, C. Veit, B. Zimmermann, F. Rauscher, P. Niyamakom, S. Yilmaz, I. Dumsch, S. Allard, U. Scherf, Efficiency enhancement for bulk-heterojunction hybrid

solar cells based on acid treated CdSe quantum dots and low bandgap polymer PCPDTBT, Solar Energy Materials and Solar Cells 95 (2011) 1232–1237.
[35] D. Celik, M. Krueger, C. Veit, H. F. Schleiermacher, B. Zimmermann, S. Allard, I. Dumsch, U. Scherf, F. Rauscher, P. Niyamakom, Performance enhancement of CdSe nanorod-polymer based hybrid solar cells utilizing a novel combination of post-synthetic nanoparticle surface treatments, Solar Energy Materials and Solar Cells 98 (2012) 433–440.
[36] T. Takagahara, K. Takeda, Theory of the quantum confinement effect on excitons in quantum dots of indirect-gap materials, Physical Review B 46 (1992) 15578–15581.
[37] S. E. Shaheen, R. Radspinner, N. Peyghambarian, G. E. Jabbour, Fabrication of bulk heterojunction plastic solar cells by screen printing, Applied Physics Letters 79 (2001) 2996.
[38] P. Schilinsky, C. Waldauf, C. J. Brabec, Performance Analysis of Printed Bulk Heterojunction Solar Cells, Advanced Functional Materials 16 (2006) 1669–1672.
[39] S. H. Eom, S. Senthilarasu, P. Uthirakumar, S. C. Yoon, J. Lim, C. Lee, H. S. Lim, J. Lee, S.-H. Lee, Polymer solar cells based on inkjet-printed PEDOT:PSS layer, Organic Electronics 10 (2009) 536–542.
[40] C. N. Hoth, S. A. Choulis, P. Schilinsky, C. J. Brabec, High Photovoltaic Performance of Inkjet Printed Polymer:Fullerene Blends, Advanced Materials 19 (2007) 3973–3978.
[41] B.-K. Yu, D. Vak, J. Jo, S.-I. Na, S.-S. Kim, M.-K. Kim, D.-Y. Kim, Factors to be Considered in Bulk Heterojunction Polymer Solar Cells Fabricated by the Spray Process, IEEE Journal of Selected Topics in Quantum Electronics 16 (2010) 1838–1846.
[42] D. Vak, S.-S. Kim, J. Jo, S.-H. Oh, S.-I. Na, J. Kim, D.-Y. Kim, Fabrication of organic bulk heterojunction solar cells by a spray deposition method for low-cost power generation, Applied Physics Letters 91 (2007) 081102.
[43] T. Matsutani, K. Yamamoto, Solvent Annealing Induced Perpendicular Orientation of Cylindrical Microdomains in Polystyrene- b -poly(4-hydroxyl styrene)/PEG Oligomer Blend Thin Film Made by Spin-coating from Selective Solvent, Journal of Physics: Conference Series 272 (2011) 012015.
[44] R. Green, A. Morfa, A. J. Ferguson, N. Kopidakis, G. Rumbles, S. E. Shaheen, Performance of bulk heterojunction photovoltaic devices prepared by airbrush spray deposition, Applied Physics Letters 92 (2008) 033301.
[45] H.-Y. Park, K. Kim, D. Y. Kim, S.-K. Choi, S. M. Jo, S.-Y. Jang, Facile external treatment for efficient nanoscale morphology control of polymer solar cells using a gas-assisted spray method, Journal of Materials Chemistry 21 (2011) 4457-4464.
[46] G. Susanna, L. Salamandra, T. M. Brown, A. Di Carlo, F. Brunetti, A. Reale, Airbrush spray-coating of polymer bulk-heterojunction solar cells, Solar Energy Materials and Solar Cells 95 (2011) 1775–1778.
[47] J. Lee, T. Sagawa, S. Yoshikawa, Morphological and topographical characterizations in spray coated organic solar cells using an additional solvent spray deposition, Organic Electronics 12 (2011) 2165–2173.
[48] W.-P. Liao, J.-J. Wu, Efficient Electron Collection in Hybrid Polymer Solar Cells: In-Situ-Generated ZnO/Poly(3-hexylthiophene) Scaffolded by a TiO 2 Nanorod Array, The Journal of Physical Chemistry Letters 4 (2013) 1983–1988.
[49] K. X. Steirer, M. O. Reese, B. L. Rupert, N. Kopidakis, D. C. Olson, R. T. Collins, D. S. Ginley, Ultrasonic spray deposition for production of organic solar cells, Solar Energy Materials and Solar Cells 93 (2009) 447–453.

[50] Y. Liang, D. Feng, Y. Wu, S.-T. Tsai, G. Li, C. Ray, L. Yu, Highly Efficient Solar Cell Polymers Developed via Fine-Tuning of Structural and Electronic Properties, Journal of the American Chemical Society 131 (2009) 7792–7799.
[51] L. Chang, H. W. A. Lademann, J.-B. Bonekamp, K. Meerholz. A. J. Moulé, Effect of Trace Solvent on the Morphology of P3HT:PCBM Bulk Heterojunction Solar Cells, Advanced Functional Materials 21 (2011) 1779–1787.
[52] G. Li, Y. Yao, H. Yang, V. Shrotriya, G. Yang, Y. Yang, 'Solvent Annealing' Effect in Polymer Solar Cells Based on Poly(3-hexylthiophene) and Methanofullerenes, Advanced Functional Materials 17 (2007) 1636–1644.
[53] J. Alstrup, M. Jørgensen, A. J. Medford, F. C. Krebs, Ultra Fast and Parsimonious Materials Screening for Polymer Solar Cells Using Differentially Pumped Slot-Die Coating, ACS Applied Materials & Interfaces 2 (2010) 2819–2827.
[54] J. Lee, T. Sagawa, S. Yoshikawa, Thickness dependence of photovoltaic performance of additional spray coated solar cells, Thin Solid Films 529 (2013) 464–469.
[55] T. J. Prosa, M. J. Winokur, J. Moulton, P. Smith, A. J. Heeger, X-ray structural studies of poly(3-alkylthiophenes): an example of an inverse comb, Macromolecules 25 (1992) 4364–4372.
[56] C. W. T. Bulle-Lieuwma, W. J. H. van Gennip, J. K. J. van Duren, P. Jonkheijm, R. A. J. Janssen, J. W. Niemantsverdriet, Characterization of polymer solar cells by TOF-SIMS depth profiling, Applied Surface Science 203 (2003) 547–550.
[57] L. Armelao, Sol–gel synthesis and characterisation of ZnO-based nanosystems, Thin Solid Films 394 (2001) 89–95.
[58] P. Sagar, P. K. Shishodia, R. M. Mehra, Influence of pH value on the quality of sol–gel derived ZnO films, Applied Surface Science 253 (2007) 5419–5424.
[59] M. Ohyama, H. Kouzuka, T. Yoko, Sol-gel preparation of ZnO films with extremely preferred orientation along (002) plane from zinc acetate solution, Thin Solid Films 306 (1997) 78–85.
[60] Y. Sun, J. H. Seo, C. J. Takacs, J. Seifter, A. J. Heeger, Inverted Polymer Solar Cells Integrated with a Low-Temperature-Annealed Sol-Gel-Derived ZnO Film as an Electron Transport Layer, Advanced Materials 23 (2011) 1679–1683.
[61] S. Chakrabarti, D. Ganguli, S. Chaudhuri, Substrate dependence of preferred orientation in sol–gel-derived zinc oxide films, Materials Letters 58 (2004) 3952–3957.
[62] Y. Natsume, H. Sakata, Zinc oxide films prepared by sol-gel spin-coating, Thin Solid Films 372 (2000) 30–36.
[63] S. O'Brien, L. H. K. Koh, G. M. Crean, ZnO thin films prepared by a single step sol–gel process, Thin Solid Films 516 (2008) 1391–1395.
[64] J. Rao, R. J. Winfield, L. H. K. Koh, S. O'Brien, G. M. Crean, Patterned transparent zinc oxide films produced by sol-gel embossing, physica status solidi (a) 205 (2008) 1938–1942.
[65] M.-S. Kim, B.-G. Kim, J. Kim, Effective Variables To Control the Fill Factor of Organic Photovoltaic Cells, ACS Applied Materials & Interfaces 1 (2009) 1264–1269.
[66] R. Brenier, L. Ortéga, Structural Properties and Stress in ZnO Films Obtained from a Nanocolloidal Sol, Journal of Sol-Gel Science and Technology 29 (2004) 137–145.
[67] Z. Liang, Q. Zhang, O. Wiranwetchayan, J. Xi, Z. Yang, K. Park, C. Li, G. Cao, Effects of the Morphology of a ZnO Buffer Layer on the Photovoltaic Performance of Inverted Polymer Solar Cells, Advanced Functional Materials 22 (2012) 2194–2201.
[68] R. D. McCullough, S. Tristram-Nagle, S. P. Williams, R. D. Lowe, M. Jayaraman, Self-orienting head-to-tail poly(3-alkylthiophenes): new insights on structure-property

relationships in conducting polymers, Journal of the American Chemical Society 115 (1993) 4910–4911.
[69] T.-A. Chen, X. Wu, R. D. Rieke, Regiocontrolled Synthesis of Poly(3-alkylthiophenes) Mediated by Rieke Zinc: Their Characterization and Solid-State Properties, Journal of the American Chemical Society 117 (1995) 233–244.
[70] H. Sirringhaus, Integrated Optoelectronic Devices Based on Conjugated Polymers, Science 280 (1998) 1741–1744.
[71] H. Sirringhaus, P. J. Brown, R. H. Friend, M. M. Nielsen, K. Bechgaard, B. M. W. Langeveld-Voss, A. J. H. Spiering, R. A. J. Janssen, E. W. Meijer, P. Herwig, D. M. de Leeuw, Two-dimensional charge transport in self-organized, high-mobility conjugated polymers, Nature 401 (1999) 685–688.

(a)

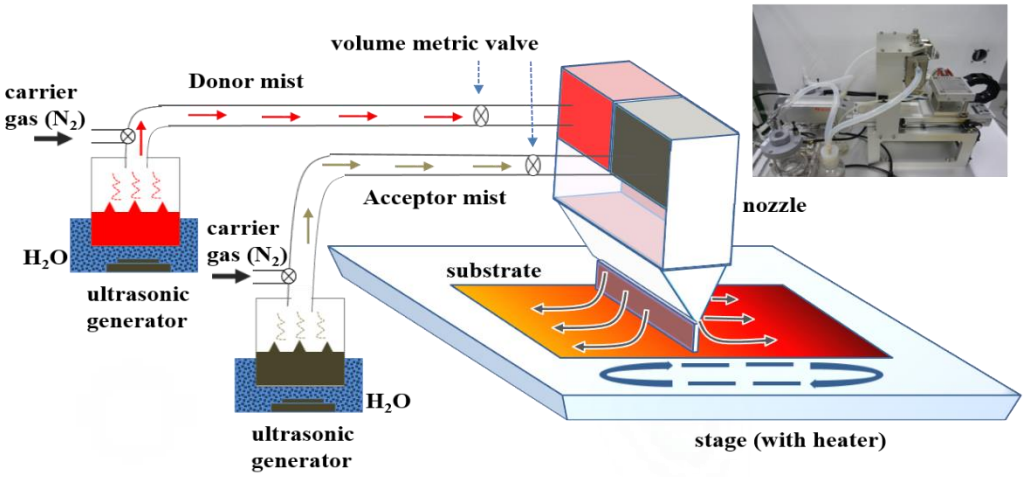

(b)

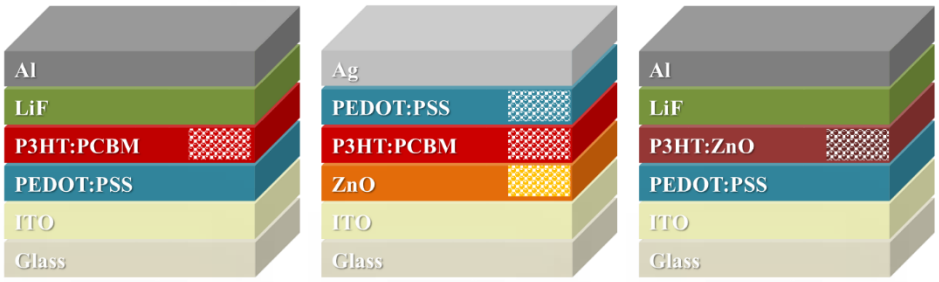

Fig. 1 (a) Schematic illustration and photograph of FCMSD apparatus. The mist from the two sources are then transferred to the nozzle by N_2 gas and combined prior to deposition to the substrate [26]. (b) the device structure of conventional, invert and hybrid type solar cell from left to right. The pattern inside a layer means fabrication by FCMSD method.

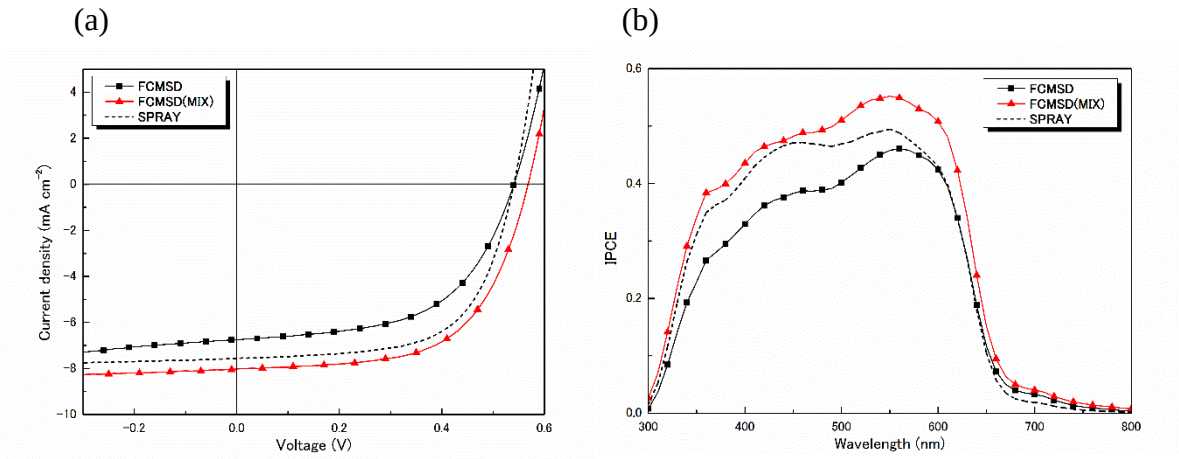

Fig. 2 (a) *J-V* characteristic of devices of glass-ITO/PEDOT:PSS/P3HT:PCBM /LiF/Al (100 mW cm^{-2}, AM 1.5G) fabricated by FCMSD, FCMSD (MIX) and spray deposition. (b) *IPCE* comparison of three devices according to coating method.

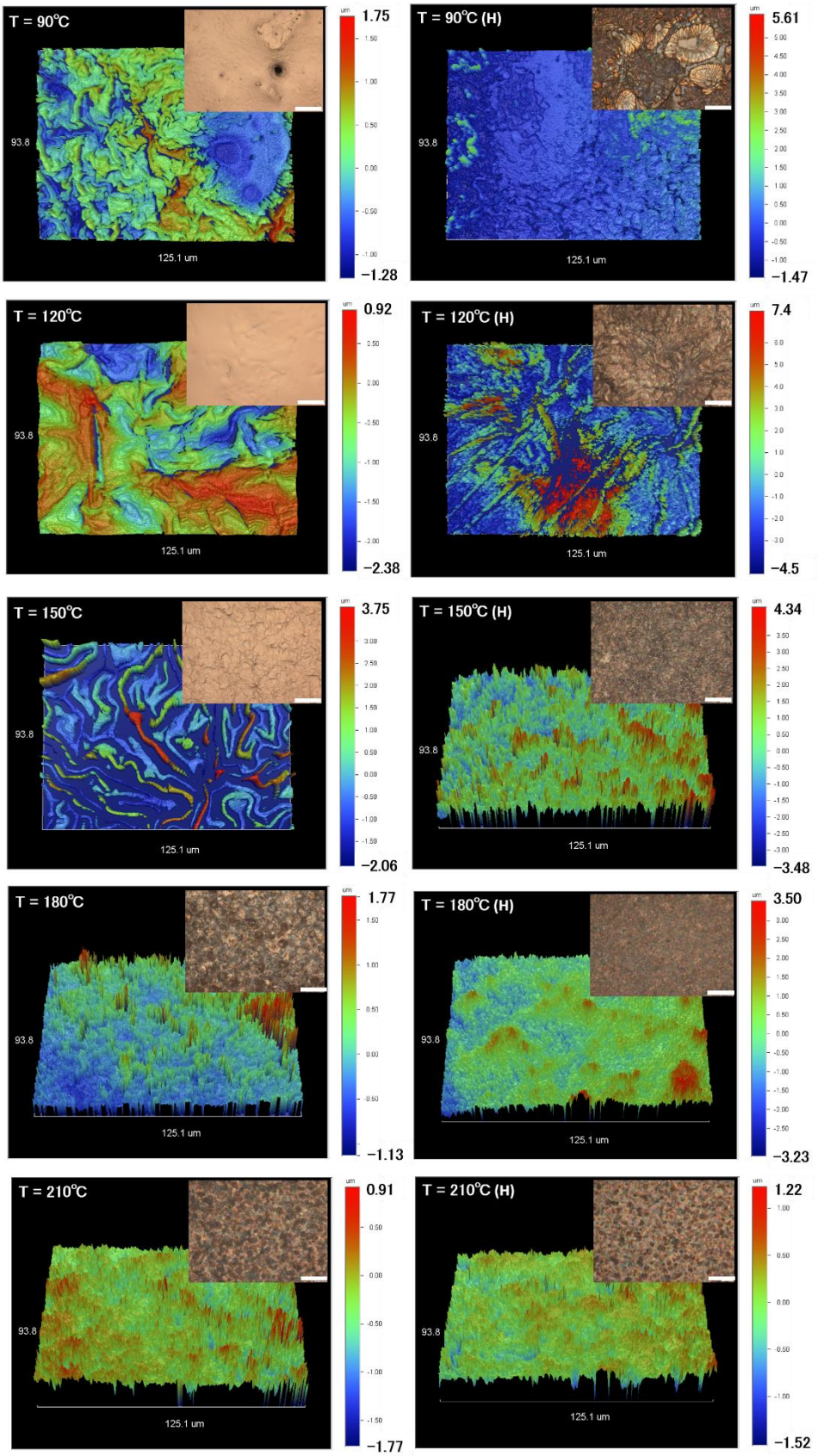

Fig. 3. Surface topographies of zinc acetate/ZnO (FCMSD) on glass substrate by surface profiler (scanning size 93.8 μm x 125.1 μm) and optical images (inset). The substrate was pre-heated at 90, 120, 150, 180 and 210 °C from top to down. All devices are investigated again after post-heat treatment (H) in right side. The bar scale of inset is 50 μm.

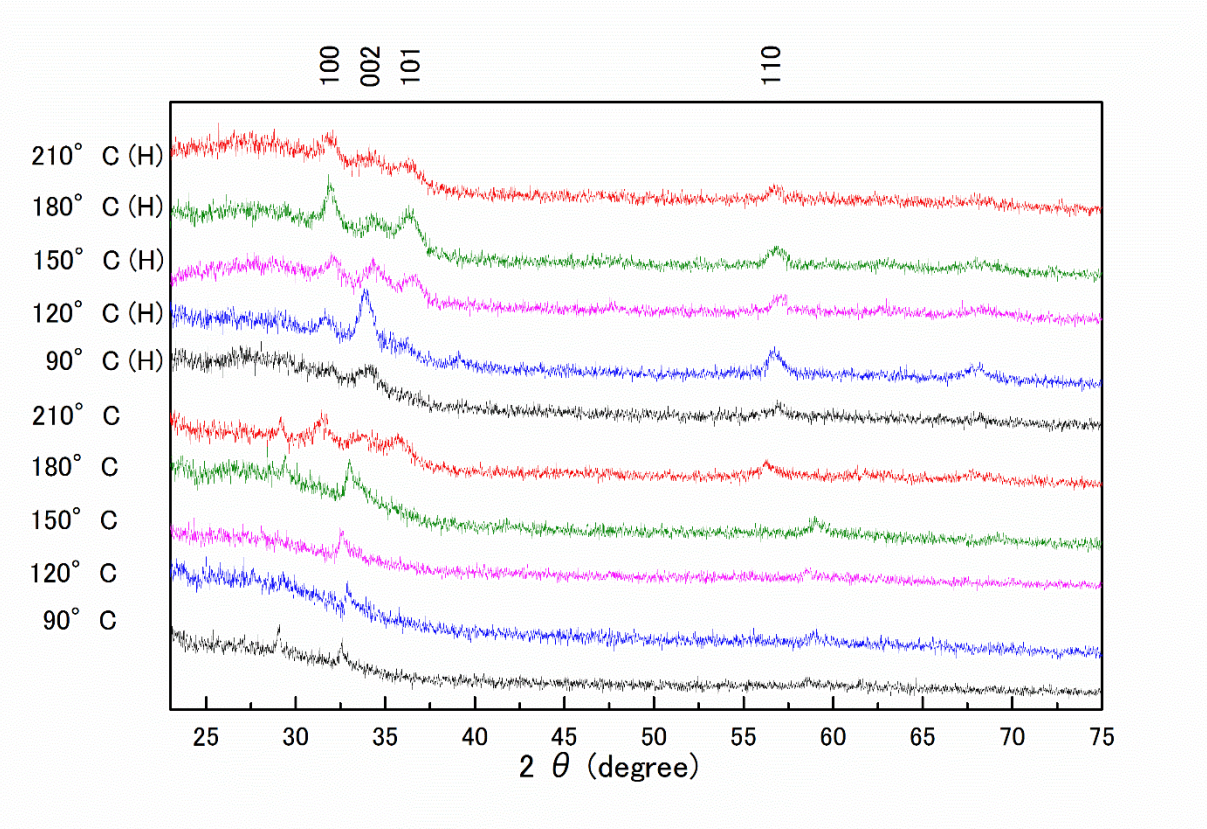

Fig. 4. XRD patterns of of zinc acetate/ZnO (FCMSD) on glass substrate by the FCMSD method. The substrate was pre-heated at 90, 120, 150, 180 and 210 °C (bottom). All devices are investigated again after post-heat treatment (H) (top).

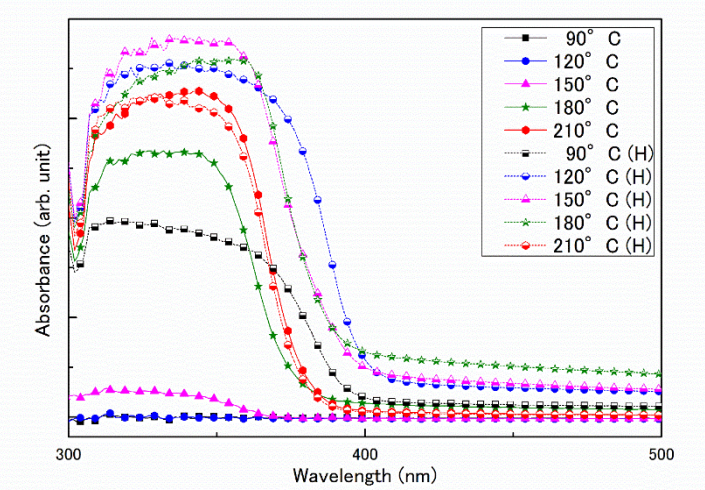

Fig. 5. UV-vis absorption spectra of zinc acetate/ZnO on glass substrate by the FCMSD method. The substrate was pre-heated at 90, 120, 150, 180 and 210 °C. All devices are investigated again after post-heat treatment (H).

(a) (b)

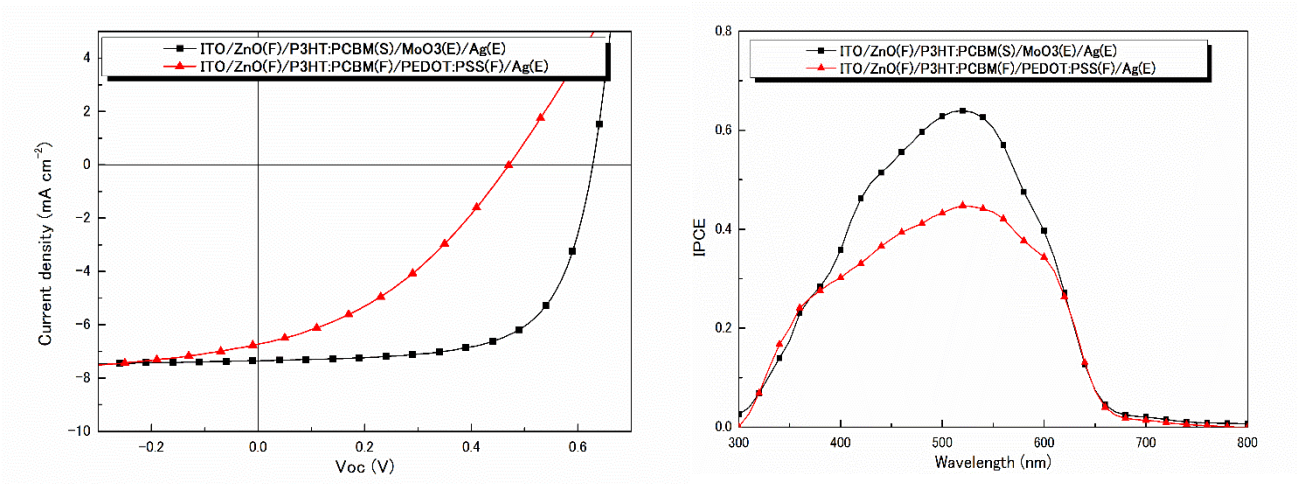

Fig. 6. (a) *J-V* characteristic, (b) *IPCE* of two inverted devices of ITO/ZnO(F)/P3HT:PCBM(S)/MoO_3(E)/Ag(E) and ITO/ZnO(F)/P3HT:PCBM(F)/PEDOT:PSS(F)/Ag(E). The abbreviation of F, S and E means FCMSD method, spin coating, evaporation respectively.

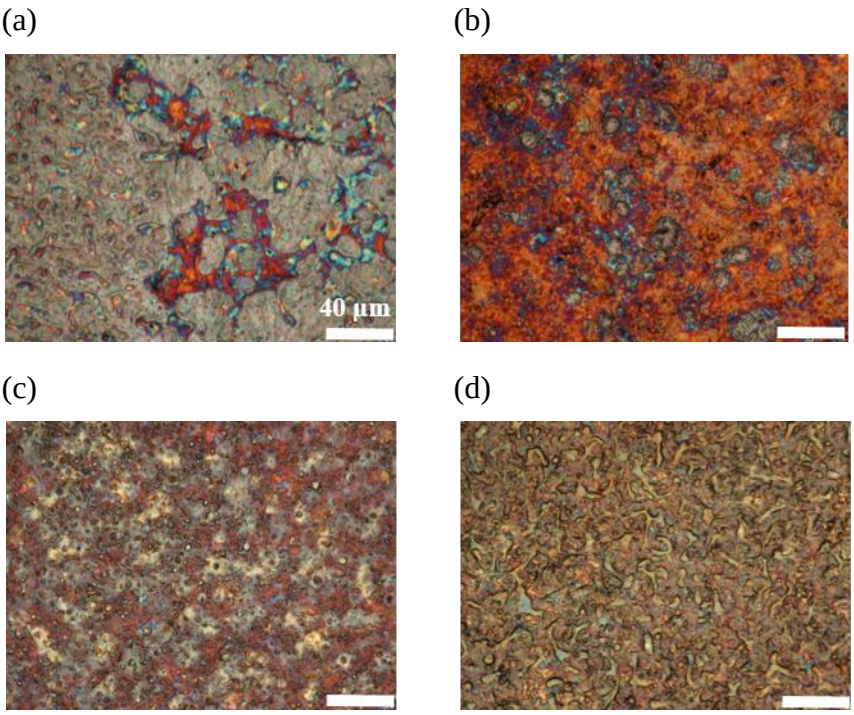

Fig. 7. Optical images of surface on the active layer (P3HT/ZnO) coated by FCMSD method. The pre-heat temperature of (a), (b) is 120 °C and that of (c), (d) is 150 °C. The image of (d) was investigated after additional solvent coating. The bar scale is 40 µm.

(a) (b)

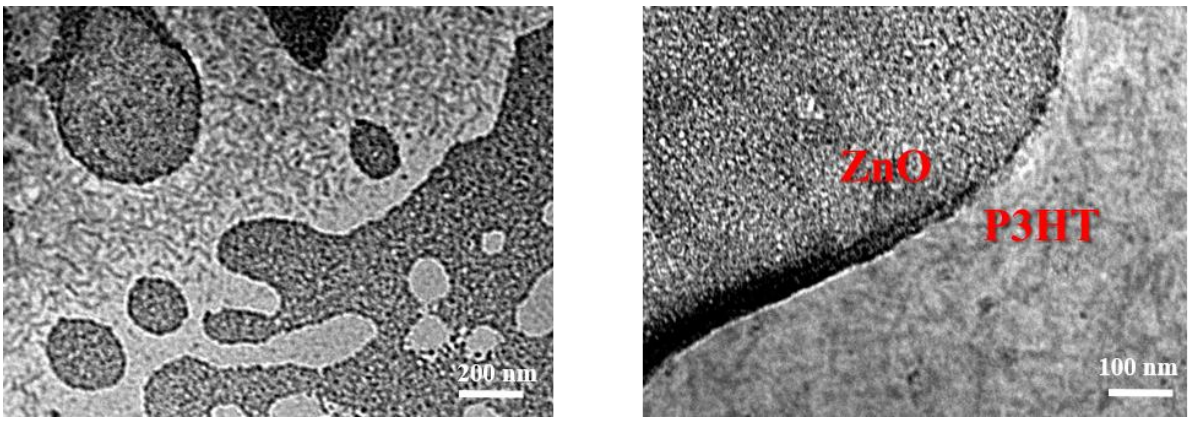

Fig. 8. TEM images of P3HT/ZnO coated by FCMSD method.

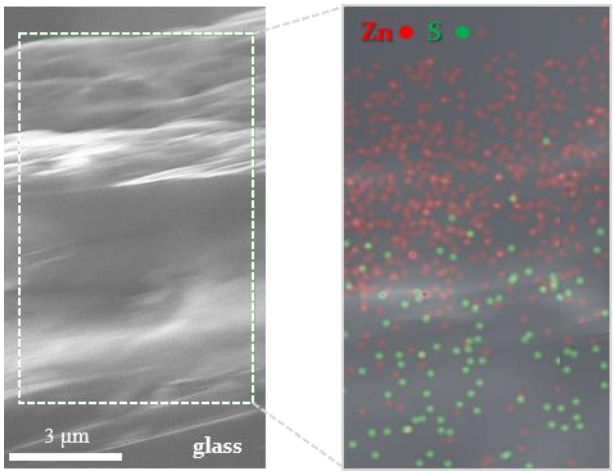

Fig. 9. EDS analyses for zinc (Zn) and sulfur (S) distributed in thicker P3HT/ZnO layer.

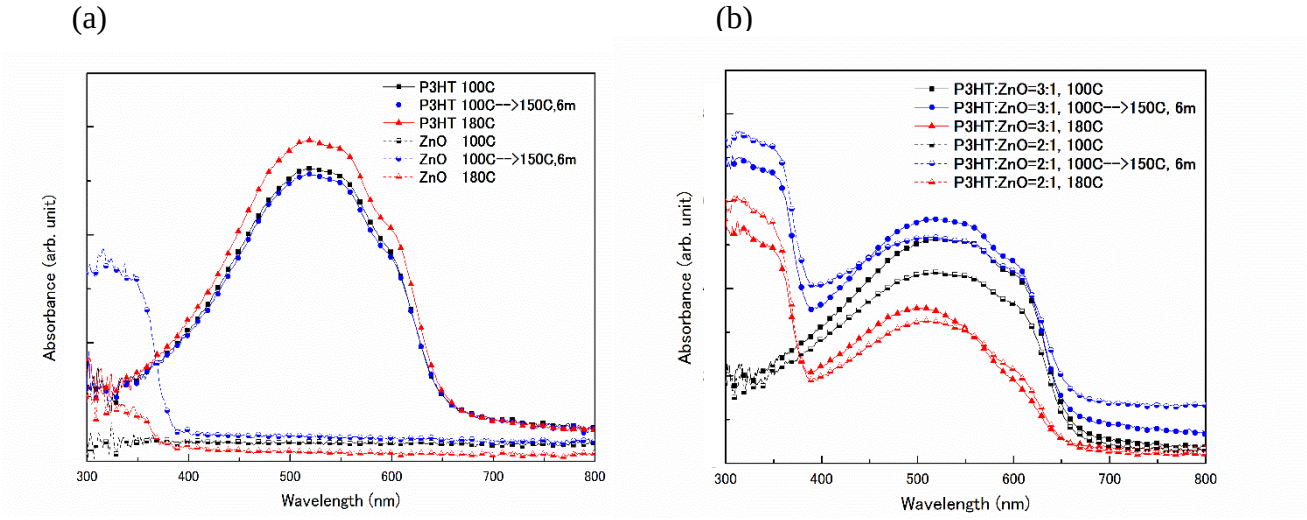

Fig. 10. UV-vis absorption spectra of (a) P3HT, ZnO and (b) the blend of P3HT/ZnO films coated by the FCMSD method. The substrates were pre-heated at 90, 180 °C. Only one device (blue line with circle) was investigated again after post-heat treatment at 150 °C for 6 min. The change as to the ratio of P3HT/ZnO is shown in (b)

Table 1. The Device performance and characteristics of glass-ITO/ ZnO(F)/P3HT:PCBM(S)/ MoO_3(E)/Ag(E) and ITO/ZnO(F)/P3HT:PCBM(F)/PEDOT:PSS(F)/Ag(E)

	E_{ff} (%)	J_{sc} (mA cm^{-2})	V_{oc} (V)	*FF*
ITO/ZnO(F)/P3HT:PCBM(S)/ MoO_3(E)/Ag(E)	3.03	7.36	0.63	0.66
ITO/ZnO(F)/P3HT:PCBM(F)/ PEDOT:PSS(F)/Ag(E)	1.19	6.73	0.47	0.38

Table 2. Current density-voltage (*J-V*) characteristics of P3HT/ZnO hybrid solar cells with different post-treatment processes.

No.	Temp. of substrate	Post-treatment			E_{ff} (%)	J_{sc} (mA cm^{-2})	V_{oc} (V)	*FF*
		Heat 1 (150 °C, 6 min)	DCB	Heat 2 (150 °C, 6 min)				
1	150°C		O		0.0012	0.0087	0.5447	0.2473
2	150°C		O	O	0.0003	0.0679	0.0172	0.2561
3	150°C	O	O		0.0300	0.3558	0.1886	0.4474
4	150°C	O	O	O	0.0233	0.3862	0.1562	0.3859